Journal of Electroceramics 1:1, 7–14, 1997

Nonstoichiometry and Electrical Conductivity of Nanocrystalline CeO_{2-x}

Y.-M. CHIANG, E.B. LAVIK, I. KOSACKI & H.L. TULLER
Dept. of Materials Science and Engineering, Massachusetts Institute of Technology, Cambridge, MA 02139

J.Y. YING
Dept. of Chemical Engineering, Massachusetts Institute of Technology, Cambridge, MA 02139

Received May 28, 1996; Revised August 9, 1996; Accepted August 16, 1996

Abstract. We synthesized dense CeO_{2-x} polycrystals of ~ 10 nm grain size and characterized their electrical conductivity, in order to determine whether the defect properties of nanocrystalline solids fundamentally differ from those of conventional materials. The nanocrystals exhibit enhanced electronic conductivity, greatly reduced grain boundary impedance, and a heat of reduction more than 2.4 eV lower per oxygen vacancy compared to their coarse-grained counterparts. We propose that defect formation at low energy grain boundary sites is responsible for these properties, and that nanocrystalline oxides represent bulk materials possessing the defect thermodynamics of interfaces.

Keywords: nanocrystals, cerium oxide, defects, interfaces, conductivity, nonstoichiometry, catalysis

Introduction

Ultrafine polycrystals with crystallite sizes in the 1–20 nanometer range have received much recent attention as materials with unique structural and physical properties [1]. Nanocrystalline oxides such as TiO_2, ZrO_2, CeO_2, and Y_2O_3 possess a particularly wide range of interesting properties including high creep deformation rates potentially useful for superplastic forming [2] and enhanced chemical reactivity useful in catalysis [3] and electrochemical sensing. All such properties fundamentally depend on the defect thermodynamics and related electrical and mass transport properties of the solid. To date, it remains unclear whether the unusual properties reported for nanocrystalline oxides are: (1) primarily the result of increased interfacial area, (2) logical extensions of conventional size scaling laws (e.g., the grain size dependence of diffusion creep [4]), or (3) the result of truly size-dependent physical properties. Terwilliger and Chiang [5] characterized the excess thermodynamic properties of fully-dense nanocrystalline compacts of TiO_2, and observed a size-dependence of the excess enthalpy which suggested deviations in the ''equilibrium''[1] defect structure. Wang et al. [6] computed the structure of nanocrystallite clusters and report a high defect concentration in the vicinity of grain boundaries. We expect that the electrical transport properties of ultrafine polycrystals should reflect any such deviations in defect thermodynamics. Electrical measurements of nanocrystalline CeO_{2-x} powders suggest a lower reduction enthalpy [7]. However, results on incompletely-densified materials are difficult to interpret due to uncertain effects from open porosity, surface adsorption, and constrictions at particle contacts. An unequivocal interpretation requires materials that can be directly compared with conventional single crystals and polycrystals.

In this study, CeO_{2-x} polycrystals of ~ 10 nm grain size (Fig. 1) and densities greater than 95% of the single crystal value have been synthesized. These are amongst the finest-grained ceramics ever prepared in bulk form. A comparison of their transport

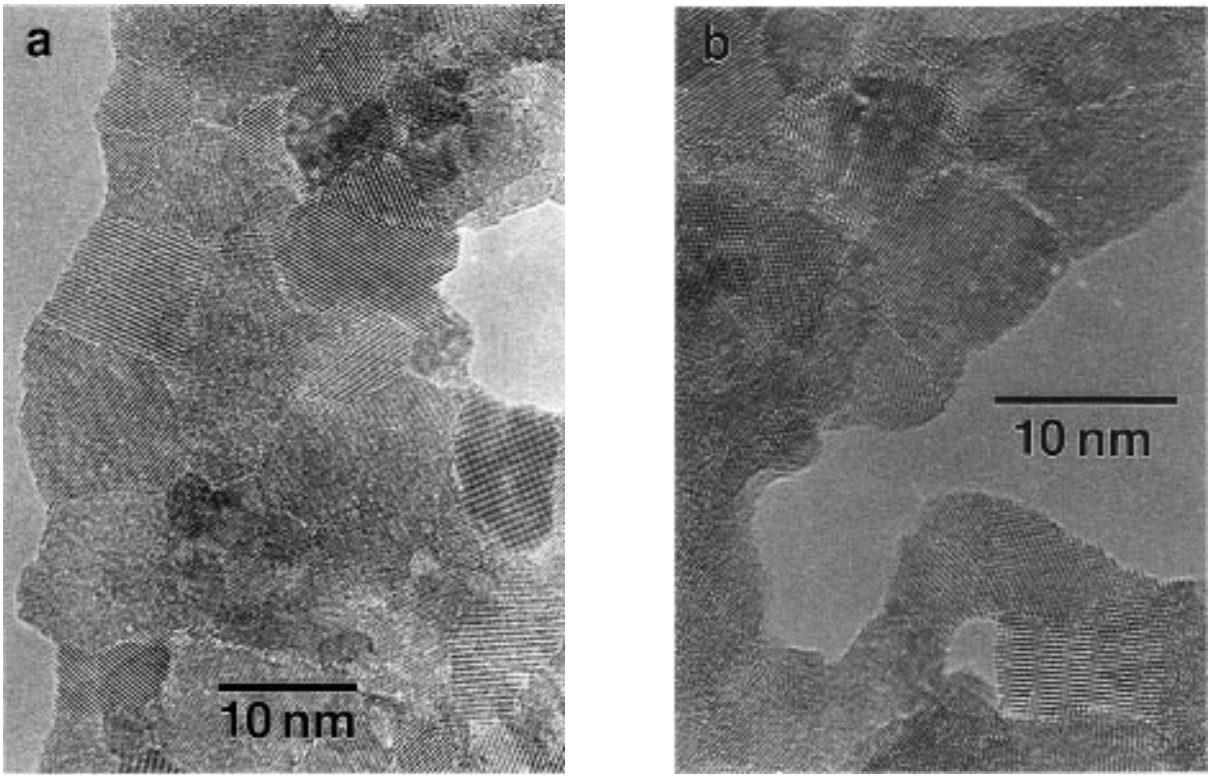

Fig. 1. HREM images of dense nanocrystalline CeO_{2-x} of 10 nm average grain diameter prepared from (a) inert-gas condensed (IGC) powder; and (b) chemically-processed (CP) powder.

properties to coarsened materials, identical except for grain size, allows an unambiguous determination of any unique behavior. A brief report of the present results appeared in reference [8].

Experimental

Two sources of CeO_{2-x} powder were used. We prepared a chemically-processed (CP) powder with a mean crystallite size of $\sim$10 nm via the decomposition of a freeze-dried cerium acetate precursor. The starting powder was analyzed by inductively-coupled plasma emission spectroscopy and found to be of very high purity, containing 40 mole ppm Si and less than 10 mole ppm of other cations. A second powder prepared by the IGC method (Nanophase Technologies Corp., Burr Ridge, Illinois) had a particle size of $\sim$5 nm and was quoted by the manufacturer as having 500 wt ppm Al and 30 wt ppm Ca. We found that it also contained several percent W, presumably originating from tungsten evaporation hardware. Nonetheless, these samples behaved almost identically to the high purity CP material, suggesting that the tungsten forms insoluble precipitates that are inert with respect to CeO_2.

Dense nanocrystalline compacts were prepared by first annealing the powders in a vacuum furnace to remove volatile surface adsorbates, then densifying at 1.1 GPa pressure and 600°C for $\sim$1 h in a tungsten carbide apparatus, forming disc-shaped samples of 6.4 mm diameter and $\sim$1 mm thickness. The densities of the samples were determined by the Archimedes method, using water as the immersion fluid. Figures 1(a) and 1(b) show high resolution electron micrographs (HREM, Topcon 002B instrument) of the exceptionally fine grain structures. A distribution of grain diameters from $\sim$3 nm to $\sim$12 nm is observed, with an average grain diameter of $\sim$10 nm. X-ray line broadening (Scherer formula) gave virtually identical values. Lattice fringes, clearly observable within most grains, meet at atomically abrupt grain boundaries with no apparent ''amorphous'' phase. Coarse-grained reference samples ($\sim$5 μm grain size) were

prepared by firing identical nanocrystalline pellets at 1200°C for 12–15 h.

For electrical characterization, platinum electrodes were applied by sputtering, and impedance spectra were obtained using a Hewlett Packard 4192-LF impedance meter operating over the frequency range 5 Hz–13 MHz, at a oscillation voltage of 50 mV. Measurements were conducted in oxygen, air, argon-oxygen mixtures, and CO/CO_2 mixtures for a range of oxygen partial pressures from 10^5 to 10^{-19} Pa. For each electrical measurement, the sample was held at the desired temperature and atmosphere until the conductivity (nonstoichiometry) stabilized. The coarse-grained samples were measured over the temperature range 500–1000°C, where they are stable against further grain growth. The nanocrystalline samples showed signs of grain coarsening at 600°C.[2] To avoid grain growth during electrical measurements, results were first collected at lower temperatures, with limited data taken at the maximum stability temperature.

Results and Discussion

The total resistances at 500°C of the nanocrystals are compared with that of a coarsened IGC sample in Fig. 2. The nanocrystals are approximately two orders of magnitude more conductive over the PO_2 range from 1 to 10^5 Pa, and furthermore, show an increasing conductivity with decreasing PO_2 characteristic of an *n*-type, reduced oxide. As discussed later, the PO_2 dependence indicates a point defect mechanism qualitatively like that in conventional CeO_{2-x} [9]. In contrast, the coarsened polycrystal exhibits a PO_2-independent conductivity which we explain as extrinsic behavior.

The impedance spectra (Fig. 3) are distinctly different for nanocrystalline and coarsened samples. The coarsened samples (Fig. 3a,c) show two arcs, characteristic of conductive polycrystals with blocking grain boundaries, including CeO_2 [10] and ZrO_2 [11], for which an equivalent-circuit consists of two RC circuits joined in series, with the bulk resistance, R_{bulk}, and grain boundary resistance, R_{gb}, being given by the intersections on the real axis of the respective semicircular arcs [11]. The dc resistivity of the coarsened samples is dominated by grain boundaries, which other studies [12,13] have shown is largely the result of impurity segregation. The coarsened IGC sample exhibits ~ 10 greater grain boundary resistivity than the CP sample despite a similar grain size ($\sim 5\,\mu$m), which we attribute to greater impurity segregation commensurate with its lower purity.

In the nanocrystalline samples, the impedance spectra (Figs. 3b and 3d) show a single distorted arc suggesting two closely-overlapping semicircles. The higher frequency ''bulk'' component of this signature may include a contribution from parallel conduction along grain boundaries, an effect that is not expected in conventional polycrystals due to the negligible cross-sectional area occupied by grain boundaries. The lower frequency ''grain boundary'' component represents conventional blocking by boundaries oriented largely normal to the current. Analysis of the latter shows that the nanocrystals have orders-of-magnitude lower boundary resistivity than the coarse-grained polycrystals. Accounting for the difference in total boundary resistance and grain size, the resistance *per grain boundary* is $> 10^3$ lower in the nanocrystals. This we attribute to grain-size-dependent impurity segregation. Recent studies in TiO_2 [14] and ZrO_2 [13] show that as grain size decreases, grain boundary impurity segregation becomes size-

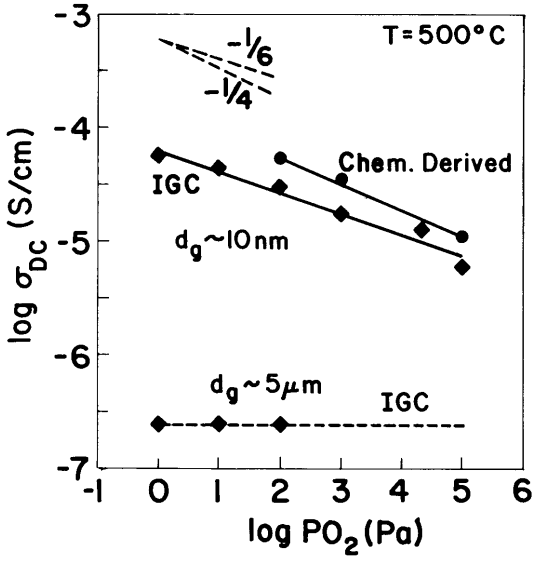

Fig. 2. Comparison of total conductivities of nanocrystalline CeO_{2-x} samples and coarsened IGC polycrystal. The nanocrystals exhibit PO_2-dependent conductivity characteristic of a reduced *n*-type semiconducting oxide, whereas the coarsened counterpart shows PO_2-independent, extrinsic conductivity.

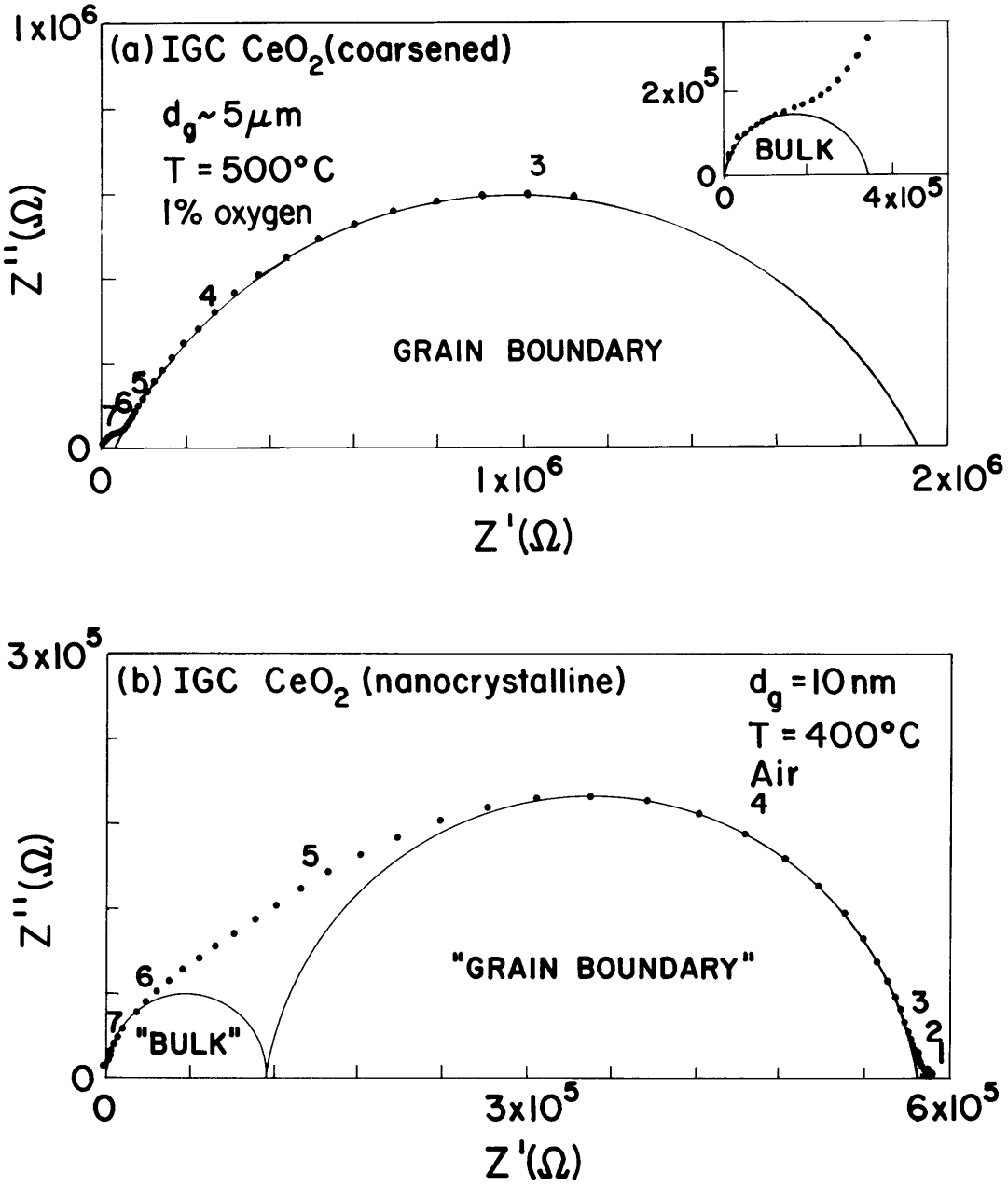

Fig. 3. Typical impedance spectra for (a) coarse-grained and (b) nanocrystalline IGC ceria, and (c) coarse-grained and (d) nanocrystalline CP ceria. Numerical labels give the logarithm of the measurement frequency (Hz).

dependent, and, in ZrO_2, determines the boundary impedance [13].

The bulk conductivities of coarsened and nanocrystalline samples, compared at 600°C in Fig. 4,[3] provide detailed information regarding defect mechanisms and thermodynamics. We expect a conductivity is given by the sum, $\sigma_{total} = \sigma_{ionic} + \sigma_{electronic}$. In the coarsened samples (e.g., Fig. 4) we observed a PO_2-independent conductivity at lower temperatures and higher PO_2, which in ceria is characteristic of extrinsic ionic conduction as a result of background acceptor impurities [15,16]. Correspondingly, measurements over a range of temperatures (not shown) yielded an activation

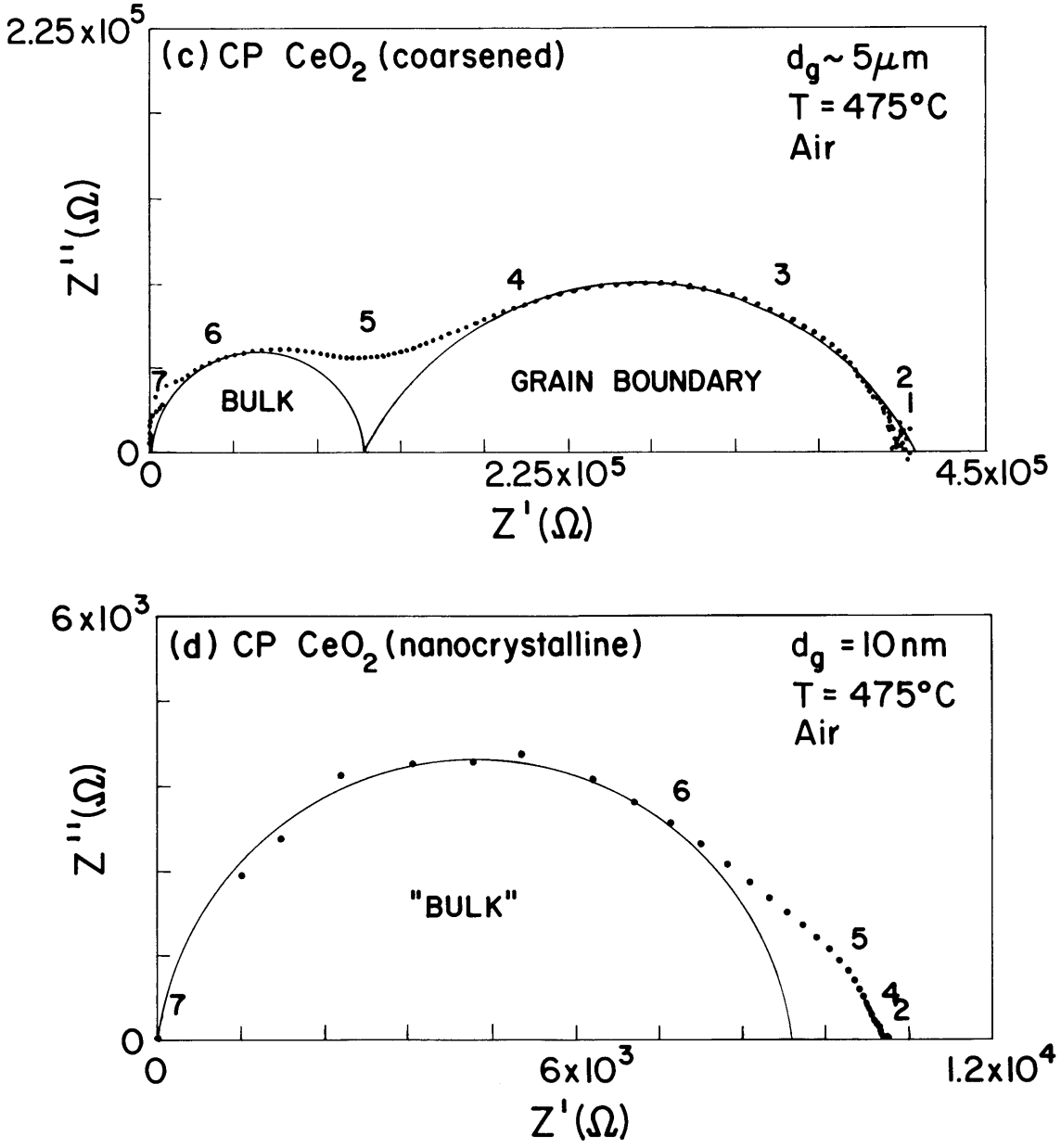

Fig. 3. (*Continued*)

energy in this regime (0.84 eV) that is close to previously reported values for oxygen vacancy migration [15,16]. At high temperatures and low PO_2, the conductivity of the coarse-grained sample becomes electronic and PO_2-dependent, following the form $\sigma \propto PO_2^{-1/m}$. The results are typical of CeO_2 with a low concentration of acceptor impurities.

In contrast, the conductivity of the nanocrystals is PO_2-dependent everywhere, and at high PO_2 is $\sim 10^4$ higher in value than the extrapolated electronic conductivity of the coarsened sample, Fig. 4. Assuming identical electron mobility μ_e in the two materials,[4] and the usual relationship $\sigma_n = ne\mu_e$, a correspondingly greater value of n may be inferred for the nanocrystal.

Proceeding further, the heat of reduction can be

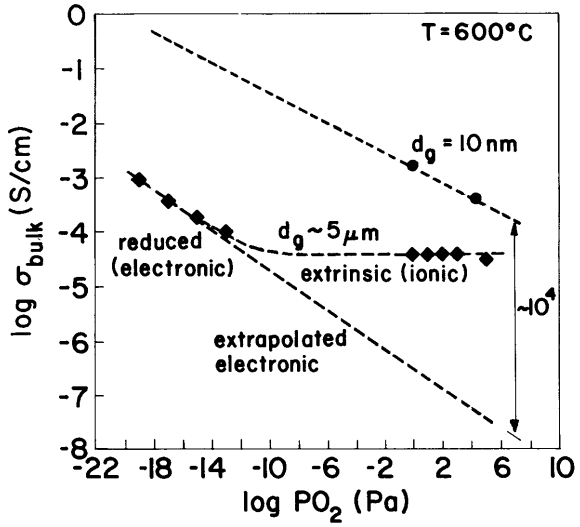

Fig. 4. The grain conductivity of the coarsened IGC polycrystal exhibits electronic and ionic regimes as a function of PO_2. In contrast, the nanocrystal conductivity follows electronic behavior characteristic of a reduced oxide throughout, and is $\sim 10^4$ greater than the extrapolated electronic conductivity of the coarsened polycrystal at 600°C.

determined from the temperature dependence of the conductivity (Fig. 5) within the respective reduced regimes. The coarsened IGC sample exhibits an activation energy of 2.45 eV, whereas the IGC and CP nanocrystalline samples exhibit significantly lower values, 0.99 and 1.16 eV respectively. These activation energies can be decomposed to obtain the heat of reduction per oxygen vacancy. CeO_{2-x} has been shown to be a classic small-polaron (hopping) conductor with a thermally activated electron mobility [21]. The electron conductivity is given by

$$\sigma_e = ne\mu_e = ne\left(\frac{\sigma_o}{T}\right)\exp\left(\frac{-E_h}{kT}\right) \tag{1}$$

wherein values for the pre-exponential σ_o and hopping energy E_h ($=0.4$ eV) were obtained in [17]. Single crystal measurements [9] show that in pure CeO_{2-x} two predominant point defects accommodate reduction at small x: doubly-ionized oxygen vacancies and electrons, formed according to the reaction:

$$O_O^x \Leftrightarrow V_O^{\bullet\bullet} + 2e' + \frac{1}{2}O_2(g) \tag{2}$$

which for dilute concentrations has the mass-action equilibrium constant

$$K_1(T) = K_1^o \exp\left(-\frac{\Delta H_1}{kT}\right) = [V_O^{\bullet\bullet}]n^2 PO_2^{1/2} \tag{3}$$

wherein K_1^0 is a constant and ΔH_1 is the enthalpy of reduction per $V_O^{\bullet\bullet}$. As we show, deviations from stoichiometry remain low under conditions attained in this study and so contributions from singly-ionized vacancies can be ignored [9]. When (2) is the dominant mechanism, electroneutrality is given by $n = 2[V_O^{\bullet\bullet}]$, a log σ − log PO_2 plot has a slope of $-\frac{1}{6}$; and a $\ln \sigma T - T^1$ plot (Fig. 5) gives an activation energy equal to

$$E_a = (\Delta H_1/3) + E_h \tag{4}$$

On the other hand, if the background concentration of acceptor impurities is large enough to pin the oxygen vacancy concentration ($[A'_{Ce}] = 2[V_O^{\bullet\bullet}]$), the equilibrium expressed in Eq. (3) still holds, the electronic conductivity should exhibit a slope of $-\frac{1}{4}$, and the activation energy is

$$E_a = (\Delta H_1/2) + E_h \tag{5}$$

From the observed activation energies (Fig. 5) we have calculated the respective heats of reduction shown in Table 1. The coarsened IGC material, which is clearly acceptor-dominated, exhibits $\Delta H_1 = 4.10$ eV using Eq. (5). This value is in good agreement with previous results for acceptor-doped

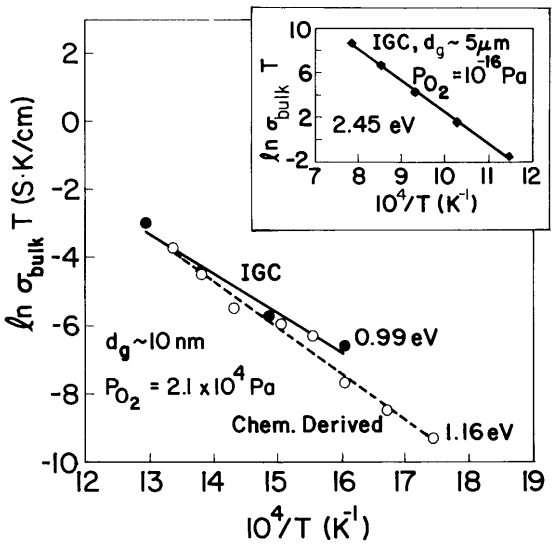

Fig. 5. The conductivity activation energy is lowered for nanocrystalline samples, indicating a lower heat of reduction. All data are from PO_2 ranges where reduced behavior dominates.

Table 1. Defect thermodynamics for nanocrystalline and coarsened CeO_{2-x}

		ΔH_1 (eV, per $V_{\ddot{O}}$)	
Sample	E_a(eV)	Intrinsic, $n = 2[V_O^{\bullet\bullet}]$	Extrinsic, $[A'_{Ce}] = 2[V_O^{\bullet\bullet}]$
Nanocrystalline, CP[a]	1.16	2.28	1.52
Nanocrystalline, IGC[b]	0.99	1.77	1.18
Coarsened, IGC[b]	2.45	—	4.10
Reduced single crystal[c]	1.96	4.67	—
Acceptor-doped polycrystals[d]	2.37	—	3.94

[a]Chemically-processed from freeze-dried cerium acetate.
[b]Inert-gas-condensation processed.
[c]From ref. 11.
[d]From ref. 18.

ceria, 3.94 eV [15]. For the nanocrystals, the PO_2 slopes (Fig. 2) are between $-1/4$ and $-1/6$. Rather than choose a single interpretation, we have calculated ΔH_1 for both intrinsic and extrinsic conditions. Assuming intrinsic reduction, Eq. (4) gives ΔH_1, for the IGC and CP nanocrystals of 2.28 and 1.77 eV respectively. These values are over 2.4 eV lower than the corresponding undoped single crystal value of 4.67 eV [9]. If an acceptor-dominated defect structure is assumed, Eq. (5) gives 1.52 and 1.18 eV respectively, again more than 2.4 eV lower than for the equivalent polycrystals.

This is a striking reduction in the vacancy formation enthalpy, which implies greater nonstoichiometry in the nanocrystals, consistent with the higher absolute value of electrical conductivity (Fig. 4). From the electron mobility at $T = 500°C$ [17], we calculate $n \approx 10^{17}$–$10^{18}\,cm^{-3}$ in the nanocrystals over the PO_2 range from 1 to 10^5 Pa (Fig. 2). Assuming intrinsic reduction, $n = 2[V_O^{\bullet\bullet}]$, the corresponding nonstoichiometry would be $x \approx 10^{-6}$–10^{-5}. While small in absolute terms, this value must be compared with that expected for a pure single crystal under the same conditions, $x < 10^{-9}$ [9]. If we assume the nanocrystals are acceptor-dominated, then the nonstoichiometry for a pure sample would be higher still. The uniqueness of the nanocrystals is that they remain reduced, with transport properties dominated by nonstoichiometry, under conditions where conventional polycrystals are clearly extrinsic.

To close, we propose an atomic-level origin for the unique defect thermodynamics. Due to the high crystalline order preserved within the nanocrystalline grains (Fig. 1) and the low absolute concentration of point defects, it is unlikely that bulk defect formation energies could be reduced by the magnitude seen here (> 2.4 eV). We propose instead that the atomic sites of lower vacancy formation enthalpy are located at grain boundaries. Preferential reduction and formation of oxygen vacancies at these sites results in the donation of electrons to the bulk which then participate in the normal small-polaron conduction process. Thus the nanocrystal is in effect doped by its own interfaces. The fraction of interface oxygen sites participating in this process can be estimated from the surface area-to-volume ratio of the nanocrystal ($S_v \approx 3/d$, where d is the average grain diameter [5]), and the average interfacial concentration of oxygen sites ($N_O^{2/3}$, where $N_O = 4.9910^{22}\,cm^{-3}$ is the density of oxygen atoms in CeO_2). At 10 nm grain size, $S_v \approx 3 \times 10^6\,cm^{-1}$, and to achieve a volume-averaged nonstoichiometry of $x = 10^{-5}$, only 10^{-4} of the available grain boundary sites need be reduced. A similar result is expected for other morphologies of equivalently high surface area-to-volume ratio, such as dispersed powders and very thin films. Thus in nanocrystalline oxides even a small fraction of interfacial sites with altered defect energetics can dominate the defect and transport behavior of the solid as a whole.

Conclusions

A direct comparison has been achieved between the electrical conductivity of dense nanocrystalline CeO_{2-x} (~ 10 nm grain size) with that of thermally coarsened counterparts ($\sim 5\,\mu$m grain size). Results show that nanocrystalline ceria possesses greatly reduced grain boundary impedance and increased

electronic conductivity, corresponding to a heat of reduction that is less than one-half its value in single crystals and conventional polycrystals. The unique defect thermodynamics, which dominate the non-stoichiometry and transport properties of the nanocrystal as a whole, are attributed to preferential reduction at grain boundary atomic sites of lowered oxygen vacancy formation energy.

Acknowledgments

We thank H. Ackler for TEM and D.A. Blom, K. Bryden, and O. Porat for experimental assistance. This work was primarily supported by the U.S. Department of Energy, Office of Basic Energy Sciences, Grant No. DE-FG02-90ER45307. Collaborations between YMC, HLT, and JYY, and Shared Facilities at MIT were supported by the National Science Foundation under award DMR94-00334. EBL acknowledges the support of an NSF Graduate Fellowship.

Notes

1. In the present context ''equilibrium'' refers to the equilibration of an oxide of fixed crystallite size with a chosen temperature and ambient gas. It is recognized that reduction in interfacial area (coarsening) represents a move towards true thermodynamic equilibrium.
2. X-ray line broadening analysis showed that the IGC sample coarsened from an average grain size of 9 nm to 11 nm after extensive electrical measurements at temperatures up to 600°C.
3. Direct comparison of nanocrystalline and coarse-grained conductivities is only possible near 600°C, since the nanocrystals coarsen rapidly at higher temperatures, while the coarsened samples do not equilibrate on the time scale of our measurements at lower temperatures.
4. While the assumption that electron mobility is unchanged in a nanocrystal is invalid in high-mobility solids where the electron mean-free path is large, and scattering from interfaces can be substantial, it is reasonable for small-polaron conductors such as CeO_{2-x}. Since the electron mean-free path is on the order of an atomic separation, significant differences in electron mobility are not expected as a function of grain size.

References

1. H. Gleiter, *Progress in Materials Science*, **33**, 1 (1990); R. Birringer, U. Herr, and H. Gleiter, *Trans. Jpn. Inst. Met.*, **27** suppl., 43 (1986); R.W. Siegel, *Ann. Rev. Mater. Sci.*, **21**, 559 (1991).
2. J. Karch, R. Birringer, and H. Gleiter, *Nature*, **330**, 556 (1987); J. Karch and R. Birringer, *Ceramics Int.*, **16**, 291 (1990); M.J. Mayo, R.W. Siegel, A. Narayanasamy, and W.D. Nix, *J. Mater. Sci.*, **5**, 1073 (1990).
3. D.D. Beck and R.W. Siegel, *J. Mater. Res.*, **7**, 2840 (1992), A. Tschoepe and J.Y. Ying, p. 781 in *Nanophase Materials: Synthesis-Properties-Applications*, G.C. Hadjipanayis and R.W. Siegel, eds., (Kluwer Academic Publ., Netherlands, 1994).
4. F.R.N. Nabarro, p. 75 in *Report of a Conference on the Strength of Solids*, (The Physical Society, London, 1948); C. Herring, *J. Appl. Phys.*, **21**, 437 (1950); R.L. Coble, *J. Appl. Phys.*, **34**, 1679 (1963).
5. C.D. Terwilliger and Y.-M. Chiang, *J. Am. Ceram. Soc.*, **78**, 2045 (1995).
6. S.R. Phillpot, J. Wang, D. Wolb, and H. Gleiter, *Mat. Sci. Eng.* A204, **76** (1995).
7. A. Tschoepe, J.Y. Ying, and H.L. Tuller, *Sensors and Actuators*. B31, 1–4 (1996).
8. Y.-M. Chiang, E.B. Lavik, I. Kosacki, H.L. Tuller, and J.Y. Ying, *Appl. Phys. Lett.*, **69**[2], 185–187 (1996).
9. H.L. Tuller and A.S. Nowick, *J. Electrochem. Soc.*, **126**, 209 (1979).
10. R. Gerhardt and A.S. Nowick, *J. Am. Ceram. Soc.*, **69**, 641 (1986), and R. Gerhardt, A.S. Nowick, M.E. Mochel and I. Dumler, *J. Am. Ceram. Soc.*, **69**, 646 (1986).
11. See for example: J.E. Bauerle. *J. Phys. Chem. Solids*, **30**, 2657 (1969); A. Ioffe, M.V. Inozemtsev, A.S. Lipilin, M.V. Perfilev, and S.V. Karpachov, *Phys. Stat. Sol. (a)*, **30**, 87 (1975), S.H. Chu and M.A. Seitz, *J. Solid State Chem.*, **23**, 297–314 (1979); N. Bonanos, B.C.H. Steele, and E.P. Butler, p.191 in *Impedance Spectroscopy*, J.R. MacDonald, ed., (John Wiley and Sons, New York, 1987).
12. M.J. Verkerk, B.J. Middelhuis, and A.J. Burggraaf, *Solid State Ionics*, **6**, 159 (1982); M. Gödickemeier et al., *J. Mat. Res.*, **9**, 1228 (1994); S.P.S. Badwal and S. Rajendran, *Solid State Ionics*, **70/71**, 83 (1994).
13. M. Aoki, Y.-M. Chiang, I. Kosacki, J.-R. Lee, H.L. Tuller, and Y. Liu, *J. Am. Ceram. Soc.*, **79**[5], 1169 (1996).
14. C.D. Terwilliger and Y.-M. Chiang, *Acta Metall. Mater.*, **43**, 319 (1995).
15. H.L. Tuller and A.S. Nowick, *J. Electrochem. Soc.*, **122**, 255 (1975).
16. R.N. Blumenthal, F.S. Brugner, and J.E. Garnier, *J. Electrochem. Soc.*, **120**, 1230 (1973).
17. H.L. Tuller and A.S. Nowick, *J. Phys. Chem. Solids*, **38**, 859 (1977).